Causes of excessive detensioning stresses in northeast extreme tee (NEXT) beams

Mauricio Diaz Arancibia and Pinar Okumus

- During prestress release, northeast extreme tee (NEXT) bridge beams crack in their flanges and webs at beam ends in recurrent patterns, which can risk bridge durability.
- The causes of flange cracks in NEXT beams were investigated in this paper using nonlinear finite element analysis that captures stress redistribution in concrete upon cracking and using field measurements of reinforcing bar strains.
- Torsion with formwork restraint and high skew angles were found to contribute the most to end cracking. Flange cutouts, flexible supports, or removable formwork are recommended for crack control.

Adjacent prestressed concrete double-tee bridge beams are favorable alternatives to adjacent box beams to cover bridge spans from 30 to 90 ft (9 to 27 m). Double-tee beams provide the same accelerated construction benefits that adjacent box beams provide. In addition, they are easy to inspect and are not prone to problems such as water accumulation in voids. In most of the northeastern United States, double-tee bridge beams are standardized and are called northeast extreme tee (NEXT) beams. They were developed based on standard double-tee beams.[1] Standard NEXT beams can be built with a precast concrete integral deck (type D) that eliminates the need for a cast-in-place concrete deck or can be built with a thinner top flange (type F) that serves as the formwork for a cast-in-place concrete deck.

Cracks have been observed at the ends of NEXT beams right after prestress release. **Figure 1** shows these cracks right after the deck placement for a type F beam. Cracks appear near the flange and web interface, running as long as 17 ft (5.2 m) along the beam's longitudinal axis. These cracks can create durability issues for bridges in harsh environmental conditions, where deicing salts can reach steel strands or reinforcement through the cracks and cause corrosion.

Although these cracks occur on both type F and type D beams, they are more pronounced for type F beams because of their thinner flanges. The flange of a type D beam can be used directly as a riding surface, and therefore both

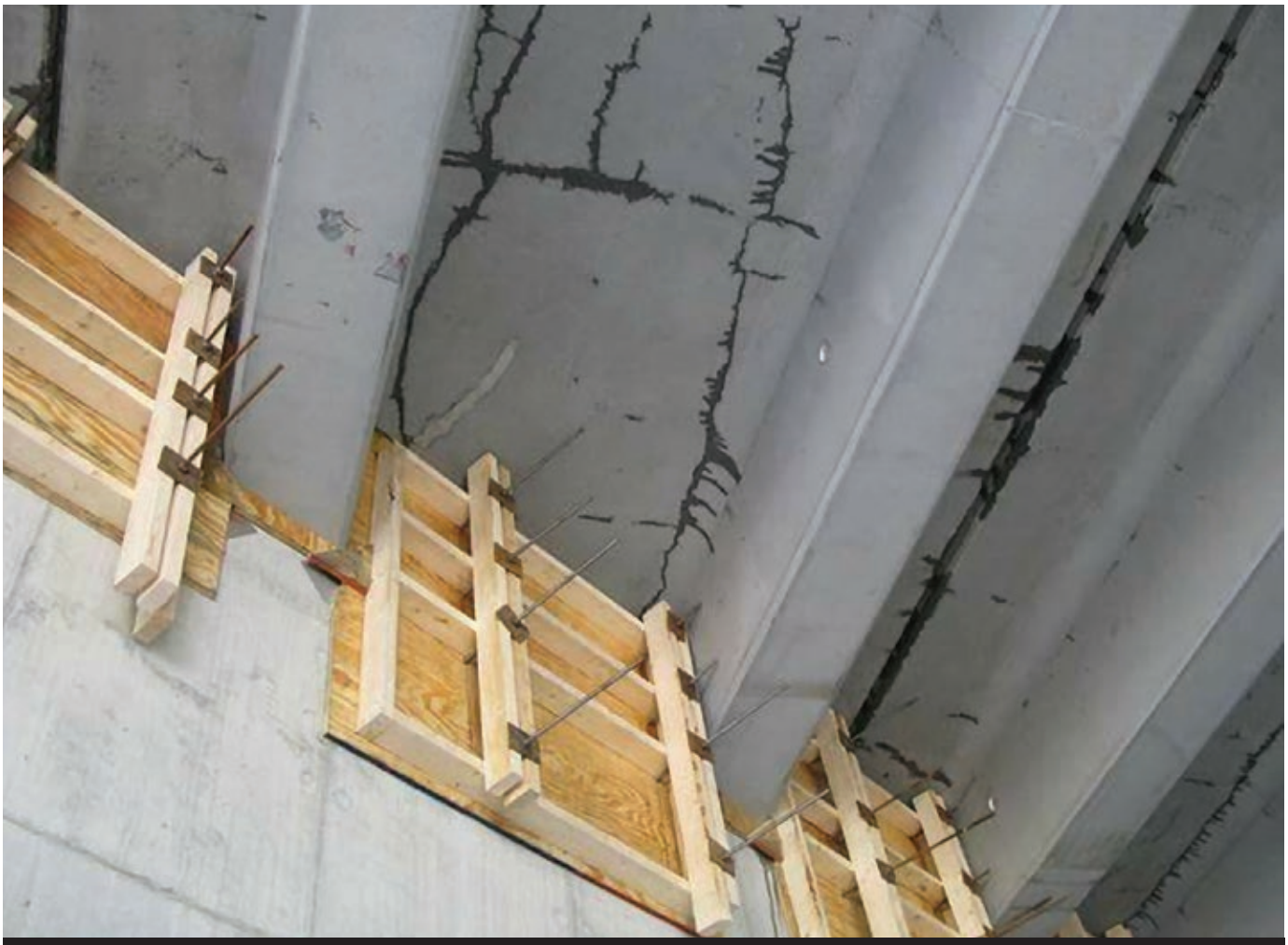

Figure 1. Flange bottom-face cracks on NEXT beam. Courtesy of Rita Seraderian, PCI Northeast.

the top and bottom faces of the flange can be permanently exposed to the environment. Such conditions warrant a thorough understanding of the extent of and reasons for cracking for both types of NEXT beams. This paper presents strain measurements during detensioning for both types of beams and investigates factors affecting cracking using analytical models of a type D beam.

Research on detensioning cracks

Cracking at detensioning has been an ongoing problem for pretensioned bridge girders, particularly for those with thin webs. Nonlinearity of girder end regions due to prestress transfer diminishes the accuracy of simple analysis methods and hinders the development of mechanics-based design methods. Simplified analysis methods,[2–4] finite element models,[4–7] and experimental methods[8–10] have been developed to explain girder end cracking and to explore crack control methods.[11,12] These studies have led to an understanding of the causes of anchorage zone cracks and possible crack control methods. However, these efforts have focused entirely on understanding and controlling end cracking resulting from prestress transfer in I-beams, bulb-tee beams,[11–13] U beams,[14] and box beams.[6]

Torsion has been reported to cause longitudinal cracks at the ends of double-tee beams used in parking structures in patterns like the one shown in Fig. 1.[15] In double-tee beams, torsion is induced by uneven supports at the ends of beams during lifting and storing or in service. Mack et al.[15] reported on industry experience with cracks, calculated torsional properties of double-tee beams, and proposed an analytical method to calculate the cracking stress based on St. Venant's torsion. Banks et al.[16] expanded the work of Mack et al. with a modified theory that combines St. Venant's torsion and flange bending, where the latter is created due to vertical forces on beam webs. This method assumes linear elasticity up to cracking and allows the prediction of the peak flange moment, bending stress at beam ends, and cracking limit.

No research has been found on end cracking of NEXT-type bridge beams. The PCI Committee on Quality Control Performance Criteria[17] published a guide for identifying and cataloging typical cracks during the production and

shipment of prestressed hollow-core slabs and double tees. This document was compiled based on field observations and experiences of PCI producer members and did not intend to quantify stresses causing cracking. Similarly, the PCI Northeast *Bridge Member Repair Guidelines*[18] lists skew, detensioning sequence, concrete binding to forms, and restrained shrinkage of the top flange by the stems as potential reasons for flange and web cracking on NEXT beams. Field observations strongly support a correlation between large beam skew angles and the severity of cracking in beam flanges. For example, the New York State Department of Transportation (NYSDOT) limits skew angles to 15 and 30 degrees for type F and D beams, respectively.[19] Factors playing a role in NEXT beam end cracking have not been analytically investigated. Cracking is likely a result of a combination of the factors listed by the PCI documents and other factors such as torsion or curing temperatures.

This study investigates the relative contributions of various factors to the likelihood and severity of NEXT beam flange cracking at beam ends. These factors include transfer of large prestress forces, restraint on the beam due to uncut strands, skew angle, temperature changes during curing, and restraint on the beam due to steel formwork.

Concrete strains and reinforcement stresses in NEXT beam end regions were investigated using three-dimensional finite element analysis. Pretensioned beam ends are shear-dominated (disturbed) regions because the transfer of prestress to concrete takes place in this region. In addition, cracking indicates that concrete does not behave elastically. Therefore, NEXT beam end behavior was investigated using nonlinear finite element analysis that considers concrete strain softening and stress redistribution to reinforcing bars upon cracking. Nonlinear modeling techniques and material models successfully used and validated in previous research[5] were employed.

In addition, two moderately skewed type D and F NEXT beams were instrumented at precasting plants to monitor strand and reinforcing bar strains and concrete temperatures during curing, detensioning, and beam lifting. Field instrumentation gave additional insights into the extent of cracking and provided a comparison to the results of the finite element analysis. Visual field inspections of NEXT beams allowed identification of typical cracking patterns expected during prestress release and lifting.

Field inspection of cracks

Precasters and departments of transportation in the northeast region have reported that after prestress release and removal of beams from formwork, NEXT beam ends crack in typical patterns. In general, two main types of cracks have been identified: flange longitudinal cracks and horizontal web cracks. The focus of this paper is on flange longitudinal cracks. Horizontal web cracks, which can be as long as 3 ft (0.9 m) and have widths that range from 0.001 to 0.005 in. (0.03 to 0.1 mm) for NEXT beams, are similar to those observed in the anchorage zones of other prestressed concrete beams, such as bulb-tee beams, and have been investigated elsewhere.[5,12,13]

Flange longitudinal cracks are located near the intersection of the flange bottom/top face and the webs, start at beam ends, and run toward the interior of the beam. The lengths and widths of these cracks are larger for beams with larger skew angles. The widths of the measured flange cracks ranges from 0.001 to 0.012 in. (0.03 to 0.30 mm). The lengths of the flange cracks ranges from 7 in. to 17 ft (180 mm to 5.2 m) for beams with skew.

Field instrumentation

To compare the finite element analysis results and to understand the extent of the stresses caused by cracks, two NEXT beams from different precasting plants were instrumented. Strains and temperatures in the end regions were monitored during prestress release and beam lifting.

Beams 1 and 2 were standard F36 and D28 NEXT beams, respectively, and were cast at different plants. Both beams had 0.6 in. (15 mm) diameter and 270 ksi (1860 MPa) ultimate strength low-relaxation prestressing strands. **Table 1** provides the essential design information for beams 1 and 2. **Figures 2** and **3** show the reinforcement details at the ends of beams 1 and 2, respectively.

Table 1. Design information for beams 1 and 2. Note: 1 in. = 25.4 mm; 1 ft = 0.305 m.

	Beam 1	Beam 2
Type	F36	D28
Length, ft	76	62
Skew angle, degrees	7.5	15
Total number of strands	50	50
Number of strands in top flange	4	4
Number of debonded strands and length	Four for 132 in. Two for 72 in.	Fourteen for 6 in. Two for 30 in. Two for 54 in. Two for 102 in. Two for 150 in. Two for 222 in.

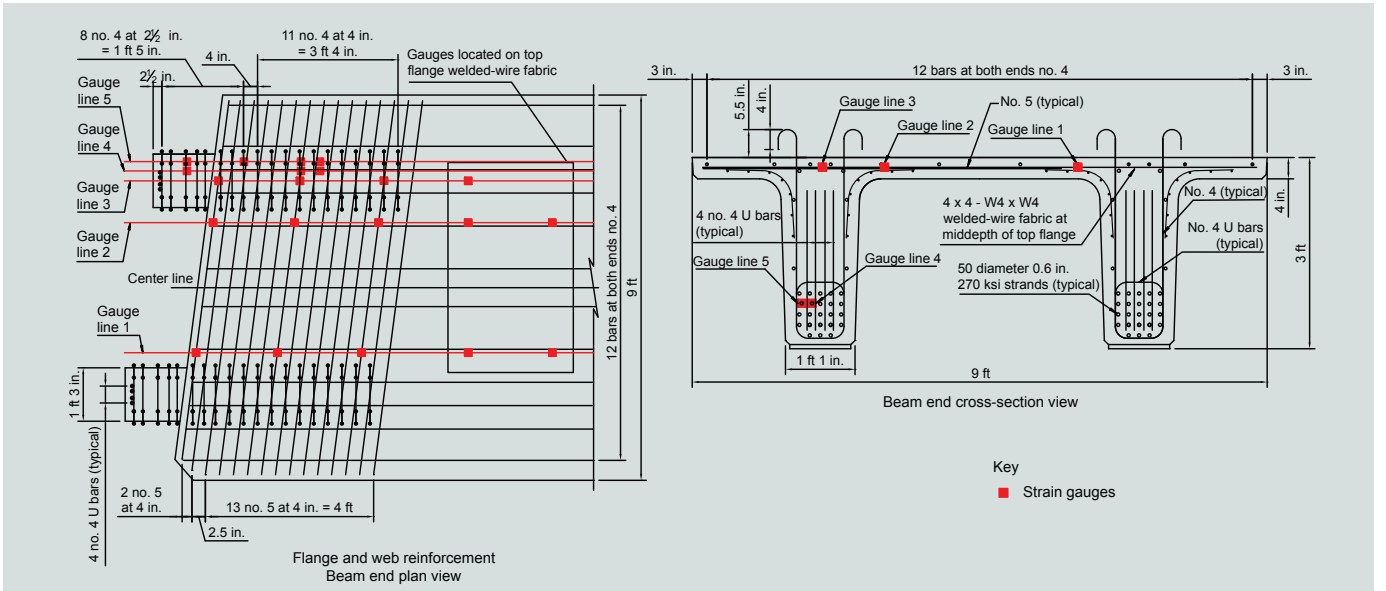

Figure 2. Reinforcement and instrumentation details for beam 1. Note: no. 4 = 13M; no. 5 = 16M; W4 = MW26; 1 in. = 25.4 mm; 1 ft = 0.305 m.

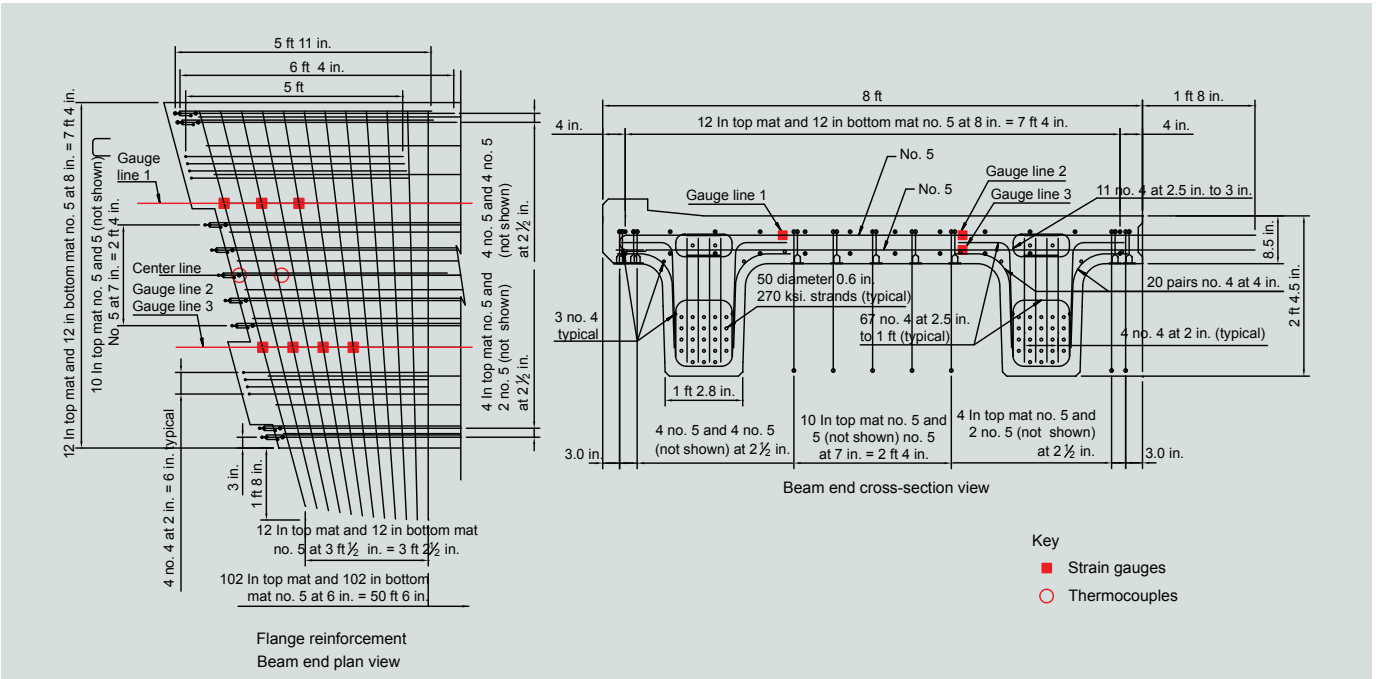

Figure 3. Reinforcement and instrumentation details for beam 2. Note: no. 4 = 13M; no. 5 = 16M; 1 in. = 25.4 mm; 1 ft = 0.305 m.

Strains were measured using surface strain gauges attached to mild reinforcement and prestressing strands. Temperature was measured using thermocouples. Strain gauges were placed close to crack-prone regions of the beam flange, based on inspections of other NEXT beams with cracks. Figures 2 and 3 show the location of strain gauges for beams 1 and 2, respectively. Additional gauges were attached to a pair of prestressing strands in beam 1 to measure prestress bond. Strain gauges on prestressing strands were placed over the transfer length, which was assumed to extend a distance equal to 60 times the strand diameter, per 5.11.4.1 of the American Association of State Highway and Transportation Officials' *AASHTO LRFD Bridge Design Specifications*.[20] Thermocouples were only installed in beam 2 and were equidistant from all strain gauges.

Instrumentation results

Prestress transfer

Figure 4 shows the strains in the prestressing strands measured discretely along the transfer length of the F36 NEXT beam (beam 1). Results along gauge lines 4 and 5 belong to an interior and exterior strand, respectively (Fig. 2). The difference in the magnitudes of strain between interior and exterior strands may be due to the dependency of prestress transfer on strand location and confinement. Auxiliary horizontal lines show the calculated strains on strands before detensioning and after elastic shortening. The average elastic shortening loss is calculated to be 17.8 ksi (123 MPa). Strand stresses after elastic shortening correlate well with the measured strains, particularly for the interior strand. Strand strain data also show that the transfer length can be approximated as 36 in. (910 mm) per the AASHTO LRFD specifications.[20] The strain data were used to extract strand-concrete bond stresses for finite element modeling.

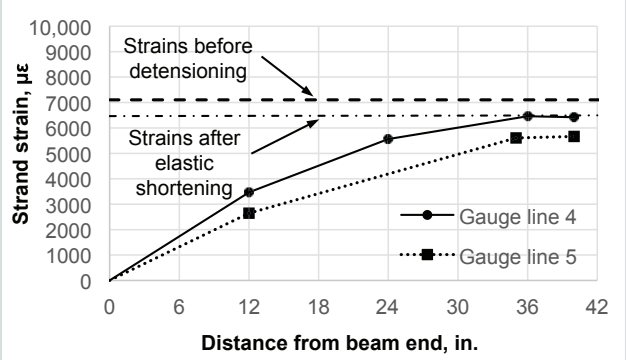

Figure 4. Strand strains right after detensioning for beam 1. Note: 1 in. = 25.4 mm.

Reinforcing bar strains due to detensioning

Mild reinforcing bar strains were measured during detensioning of beams 1 and 2 and during lifting of beam 1. **Figure 5** shows the variation of strains presented along gauge lines parallel to the longitudinal cracks.

Beam 1: F36 NEXT beam The black lines on Fig. 5 (left) show strains due to detensioning for beam 1 for gauge lines 1, 2, and 3 (Fig. 2). High transverse tensile strains at the beam end rapidly decrease within 24 in. (610 mm) of the beam end with increasing distance from the end. Higher strains shown on gauge lines 1 and 2 seem to reflect flange bottom-face crack patterns near the acute and obtuse corners of the beam, respectively. The high transverse tensile strains at the beam end along gauge line 3 indicate flange top-face cracks, though these cracks were not visible to the naked eye as the top surface of the beam was roughened for composite action.

The red lines on Fig. 5 (left) present changes in strains due to beam lifting for gauge lines 1, 2, and 3 of beam 1. Along gauge line 1, change in compression strains due to lifting increased into the beam. Change in compression strains along gauge lines 2 and 3 were the highest between the end of the beam and the location of the lifting hoop at 24 in. (610 mm) from the beam end.

Beam 2: D28 NEXT beam Figure 5 (right) also presents the measured strains for beam 2 along gauge lines 1, 2, and 3 (Fig. 3). Gauges located along gauge line 3 had the highest strains. At the beam end, the transverse tensile strains on reinforcing bars decrease with increasing distance from the end. Gauge lines 1 and 2 had negligible tensile or compression strains. Small strains were expected for gauge line 2 because no cracks formed near this gauge line.

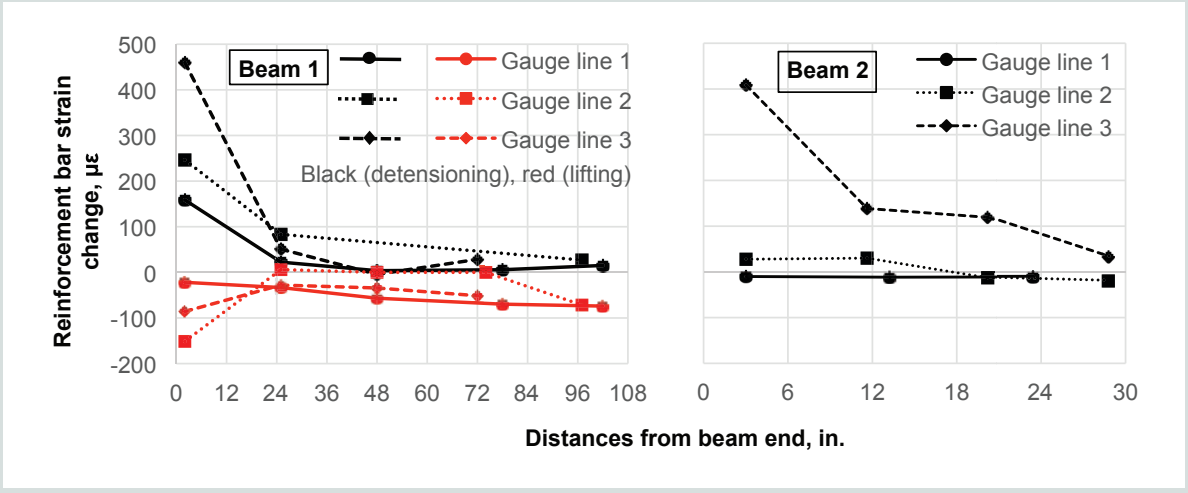

Figure 5. Reinforcement bar strain changes due to detensioning for beams 1 and 2 and due to beam lifting for beam 1. Note: 1 in. = 25.4 mm.

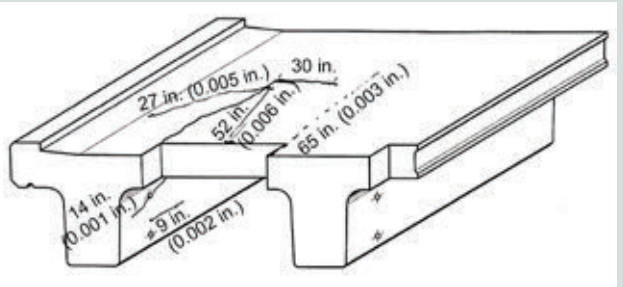

Figure 6. Crack map for instrumented end of beam 2. Courtesy of L. C. Whitford Materials Co. Inc. Note: 1 in. = 25.4 mm.

Alternatively, gauge line 1 strains were smaller than expected, as the flange top face cracked (**Fig. 6**) closer to the acute corner of the beam. This may be due to the misalignment of the selected locations of the gauges and the crack, the shallow crack not reaching the reinforcement during detensioning, the reinforcement not being parallel to principal tensile concrete strains, or cracking developing during lifting. Measurements showed that concrete temperatures went from 86°F to 176°F (30°C to 80°C) during curing. Temperature changes over detensioning were negligible (-1.4°F [-0.78°C]). Figure 6 shows the crack map for the instrumented end of beam 2. This map was created after the beam was lifted from the casting bed.

The results of field instrumentation showed that for types F and D beams with skew angles of less than 15 degrees, reinforcing bar strains did not exceed 500×10^{-6} and decreased below the cracking limit within 2 ft (0.6 m) of the girder end. This distance is shorter than the lengths of the cracks observed on the beams.

Finite element analysis

Finite element analysis was used to identify the relative contributions of various design and construction factors to NEXT beam end cracks. Using finite element analysis software, beam 2 was first modeled under prestress and gravity loading only. This model is called the baseline model. The baseline model was then modified with varying parameters and boundary conditions to understand the field of tensile strains that cause cracking during prestress release. Properties of finite element analysis used to build the baseline model—and critical for describing the work—are given in this section. Additional information on the details of finite element analysis techniques can be found elsewhere.[5]

Boundary conditions

The beam cross section at midspan had symmetry boundary conditions to reduce analysis run time. At midspan, only translation along the longitudinal axis of the beam was restrained. In addition, sag of the beam due to gravity was prevented by defining non-friction, hard contact between the bottom face of beam webs and formwork. A complete formwork was also incorporated into select models using the same modeling technique. This contact interaction allows free separation of the beam and the formwork when the beam cambers under prestress. Formwork was defined as an analytical rigid surface to further reduce computation time.

Loading

Because cracks occur right after detensioning, beam self-weight and prestress loads were the only loads included in the models. Prestress loads were applied following the strand cutting order used by the precaster of beam 2 (that is, from top to bottom and exterior to interior strands). Prestress was applied after gravity force was activated. Transfer of prestress was simulated by directly applying shear traction on the concrete around the diameter of strands along the predicted transfer length. Bond stress distribution was inferred from the strand strain measurements at transfer (Fig. 4).

Material linearity

Concrete nonlinear properties were only assigned to the region of beams where cracks were expected to develop (that is, the beam end) to reduce model run time. This region extends into the beam for a distance approximately equal to the largest dimension of the beam cross section from the end per St. Venant's principle. Linear elasticity was assumed for the rest of the concrete beam away from the ends, for mild reinforcement, and for prestressing strands, when included.

Mild reinforcement was only defined for the nonlinear concrete region. The interaction between mild reinforcement and concrete was modeled using the embedded element technique. In this approach, the translational degrees of freedom of reinforcement are constrained by the response of the surrounding concrete. Slip of reinforcing bars in concrete is indirectly modeled through tension softening in concrete.

Material properties

Concrete material properties were based on a concrete damaged plasticity model. The material property input for concrete was constructed based on the constitutive models provided by the fib *Model Code for Concrete Structures 2010*[21] for nonlinear behavior of concrete and the AASHTO LRFD specifications[20] for linear behavior of concrete. In compression, concrete was assumed to remain linear up to 40% of the compressive strength. In tension, the limit of linearity for concrete was calculated per C5.4.2.7 of the AASHTO LRFD specifications. Linear elastic properties of mild reinforcement steel were defined per 5.4.3.2 of the AASHTO LRFD specifications.

Finite elements

Concrete was modeled using three-dimensional, linear, eight-node, hexahedral elements with reduced integration. Mild steel reinforcement was included in the models as three-dimensional, linear, two-node truss elements.

Mesh sensitivity analysis required the use of a global mesh size of 1 in. (25 mm) for the nonlinear concrete region and linear mild reinforcement. The linear elastic portion of concrete has the mesh size gradually varying from 1 to 4 in. (25 to 100 mm) with increasing distance from the beam end.

Verification of the baseline finite element model results

Stresses and deflections obtained by finite element analysis of the baseline model were verified by comparing them with analytically calculated counterparts where an analytical solution was available. The closed-form solution based on the linear-elastic beam theory is valid and accurate for the midspan, where the behavior is linear elastic.

Table 2. Comparison of finite element analysis and analytical results for the baseline beam model

Stress or deflection	Finite element analysis	Analytical	Finite element analysis/ analytical
σ_{bottom}, ksi	-3.756	-3.582	1.05
σ_{top}, ksi	-0.142	-0.142	1.00
Δ, in.	1.739	1.855	0.94

Note: Δ = beam deflection; σ_{bottom} = bottom-fiber concrete bending stress; σ_{top} = top-fiber concrete bending stress. 1 in. = 25.4 mm; 1 ksi = 6.895 MPa.

Table 2 compares the bottom-fiber concrete bending stress σ_{bottom}, top-fiber concrete bending stress σ_{top}, and deflections Δ of beam 2 as obtained by linear finite element analysis and as calculated by the beam theory.

Analytical calculations were performed using transformed cross sections. Positive stresses indicate tension, and positive deflections indicate an upward direction. Table 2 shows that the differences between the finite element analysis and analytical results are within 6% of each other and within acceptable limits.

Factors contributing to end-zone cracks

Finite element analysis models were used to understand the isolated or combined contribution of various factors to end-cracking strains to identify causes of cracking. These factors include:

- prestress
- restraint by uncut strands
- skew angle
- thermal loads
- restraint by formwork

The results of models for each factor are given in this section.

Prestress (baseline model)

Similar studies[5] on the end-zone cracking behavior of deep bulb-tee beams showed that cracks during detensioning were mainly caused by prestress forces. Based on this experience, the baseline model of beam 2 considered only self-weight and prestress. **Figure 7** shows contour plots of principal

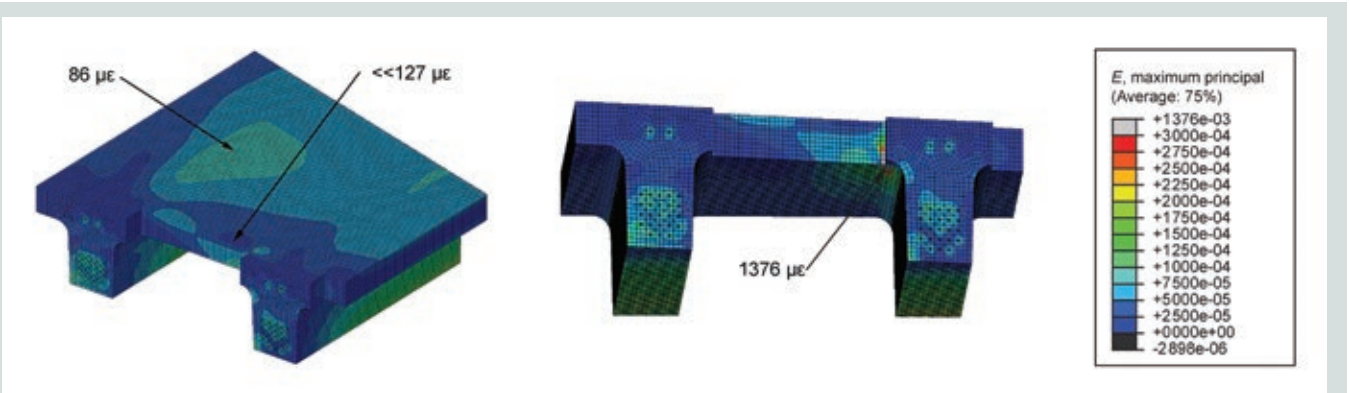

Figure 7. Principal tensile strains under prestress in units of microstrain.

tensile strains at the beam end. The magnitudes of maximum principal tensile strains on flange top and bottom faces are also shown. Figure 7 shows that tensile strains on the flange top face close to the acute corner of the beam did not exceed the theoretical concrete cracking strain (that is, 127×10^{-6}). Hence, cracks were not predicted in this region. In addition, the model predicted that if cracks existed they would initiate at approximately 3.5 ft (1.1 m) from the beam end and propagate longitudinally in both directions. Alternatively, Fig. 7 also displays tensile strains well above the theoretical concrete cracking strain for the flange bottom face closer to obtuse corner. Such a result suggested that cracks initiated at the end and propagated toward the interior.

Restraint by uncut strands

Prestress is commonly released by flame-cutting strands according to a specific cutting order. Therefore, during detensioning, beam deformations caused by detensioned strands can be temporarily restrained by uncut strands. This restraint can cause tensile strains and cracking at the web-flange interface and was investigated.

The baseline model was modified to include the restraining effect of uncut strands during detensioning. Restraint due to uncut strands was modeled by including three-dimensional strand elements in the models for uncut strands. Linear, eight-node, hexahedral elements with reduced integration were used for prestressing strands. Prestressing strand geometry was simplified, and strands had circular cross sections. Prestress bond was modeled by assigning mechanical contact between the strands and the surrounding concrete based on friction. The friction coefficient was calibrated to be 0.3 using test data in Fig. 4. Due to the excessive computational cost of this modeling technique, only strands located in the top flange and their restraint were included in the model.

The inclusion of the restraining effect of top strands caused minor changes in the strain field. Approximate increases of 10% and 4% from the baseline model strain values (Fig. 7) were observed on flange top and bottom faces, respectively. High tensile strains on the flange top face extended toward the obtuse corner of the beam, but their magnitude remained below the theoretical concrete cracking strain.

Skew angle effects

Precast concrete manufacturers observe that beams with higher skew angles are more prone to cracking. To investigate the link between skew angle and detensioning cracks, the baseline models were re-created with 0-, 15-, 30-, and 45-degree skew angles. The skew angle limit[19] for type D NEXT beams was intentionally exceeded. **Figure 8** presents the change in concrete principal tensile strains in the end region with increasing skew angles. Maximum principal tensile strain magnitudes are highlighted.

Figure 8 shows that for a beam with a 0-degree skew angle, the highest tensile strains are on the interior bottom faces of the flange. With no skew and for the level of prestress on this beam, the theoretical cracking strain of concrete (that is, 127×10^{-6}) was not exceeded.

Flange top-face strains do not increase considerably with skew and they peak at a distance of 3 to 5 ft (0.9 to 1.5 m) into the beam. Top flange cracks, therefore, are likely caused by other factors. Figure 8 also shows that with increasing skew angles, tensile strains in the intersection of the flange bottom and web increase on the obtuse side. Even with a 15-degree skew angle, principal tensile strains far exceed the theoretical concrete cracking strain, indicating the formation of a crack. Strains rapidly decrease to magnitudes below the theoretical cracking strain with increasing distance along the beam, at approximately 30, 60, and 65 in. (760, 1500, and 1650 mm) for 15-, 30-, and 45-degree skew angles, respectively. As discussed while describing the finite element analysis technique, strains above the theoretical cracking limit qualitatively indicate crack width, due to the stress-crack opening relationship used to define concrete tensile properties.

The maximum reinforcing bar stresses were 0.9, 4.6, 17.1, and 22.6 ksi (6, 32, 118, and 156 MPa) for 0-, 15-, 30-, and 45-degree skew angles, respectively. All maximum reinforcing bar stresses were in the interior side of the webs on the flange bottom face at the obtuse corner. Both transverse bars in the flange and curved bars at the flange–web intersection had high stresses, indicating that these reinforcing bars are effective for crack control. Curved welded-wire reinforcement remained perpendicular to the longitudinal axis of the beam and, therefore, was slightly less effective than the transverse flange bars that were placed parallel to the skew angle. Reinforcing bar stresses exceeded one-third of the yield strength of reinforcing steel (20 ksi [140 MPa]) for a 45-degree skew angle, indicating that additional reinforcement may be required to control crack width for a 45-degree skew angle.

Thermal effects

Temperature changes may cause strains in concrete due to the difference between the thermal properties of steel and concrete.[22] In addition, volumetric changes such as the ones created by curing temperatures can lead to nonuniform deformations in beams with skew. The longitudinal deformations can be distorted as the largest deformations are expected along the longer diagonal axis between the acute corners of beam ends. The possibility of thermal changes causing tensile strains and cracking was investigated by adding a temperature change representing the

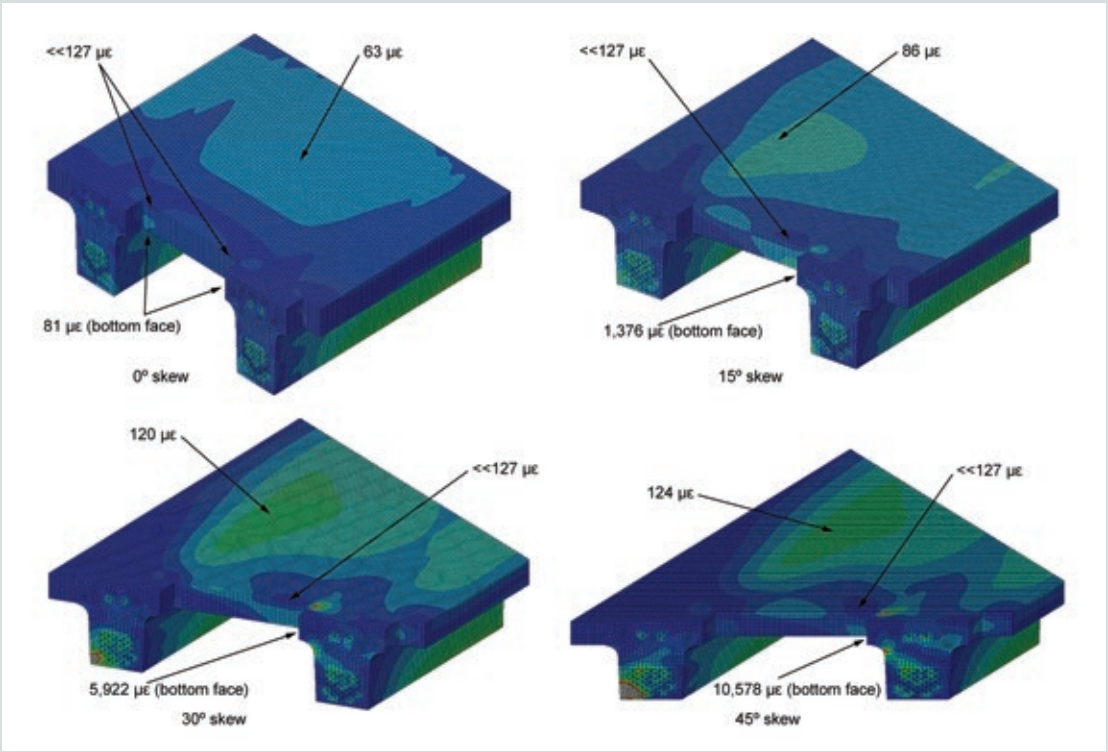

Figure 8. Top- and bottom-face principal tensile strains with varying skew angles in units of microstrain.

curing temperatures to the baseline model prior to prestress release.

A coupled thermal-stress analysis was run in which concrete was modeled using three-dimensional, linear, eight-node, hexahedral elements with reduced integration. Mild reinforcement was modeled with three-dimensional, linear, two-node truss elements. Thermal properties for concrete and mild reinforcement were taken from 5.4.2.2 and 6.4.1 of the AASHTO LRFD specifications,[20] respectively. Temperature measurements during casting of beam 2 revealed that steam curing can cause up to a 90°F (50°C) increase in internal concrete temperature: 86°F (30°C) and 176°F (80°C), respectively. Measurements also showed that temperature could be assumed constant during prestress release. For simplicity and conservatism, concrete was assumed to harden seven to eight hours after placement. This corresponds to an internal temperature increase of 54°F (30°C) between hardening and detensioning. These models yielded strain results practically identical to those of the baseline model and are not shown here, indicating curing temperatures do not play a major role in cracking.

Restraint by formwork

NEXT beams are cast in a single-piece formwork and are detensioned while they are still restrained by steel formwork on all surfaces, unlike bulb-tee girders, which have the sides of the formwork removed before detensioning. When NEXT beams camber up due to prestress, beams may become temporarily supported on the flange bottom face by the formwork alone. Similarly, beam stems may become temporarily and partially unsupported. This support condition could promote the formation or propagation of cracks. Flange cutouts at the beam end may reduce or eliminate the described effect.

To simulate this effect, the baseline model was altered to include a non-friction, hard-contact interaction between the NEXT beam and a complete formwork. All surfaces of the steel formwork were included as analytical rigid surfaces.

Figure 9 shows major differences in the simulated end-beam behavior due to restraint by formwork and due to prestress only. The magnitude of tensile strains on the flange top face in the region close to the acute corner exceeded the theoretical concrete cracking strain, with maximum values at the beam end. Tensile strains in the flange bottom face on the obtuse corner also increased by 80% compared with the strains in the baseline model. For both regions, tensile strains exceeding the cracking strain were observed as far as 3 ft (0.9 m) from the girder end. Finally, the strain results in Fig. 9 imply a cracking pattern that resembles the one observed for the instrumented NEXT beam in Fig. 6. Differences in crack patterns observed in

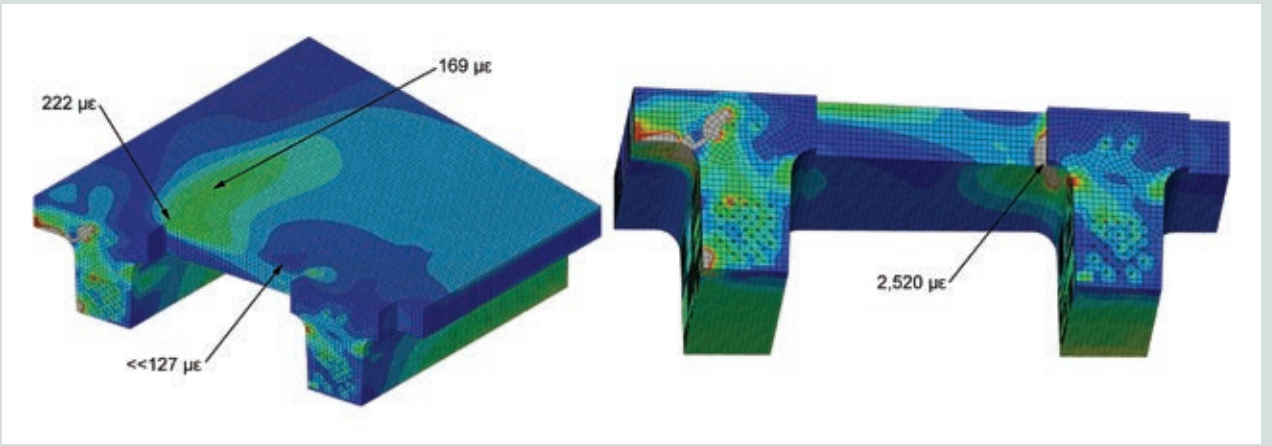

Figure 9. Principal tensile strains under restraint by formwork in units of microstrain.

the finite element analysis and Fig. 6 are likely due to the effects of lifting, which were not included in the finite element analysis.

Differential camber between webs

On beams with skew, there is a difference in camber between the centerlines of the stems at any given cross section perpendicular to the beam axis. This difference (**Fig. 10**, right), causes torsional deformations and tensile strains on the top flange near the acute and obtuse corners.

Because formwork restraint also plays a role in differential camber between stems, this effect was captured using the finite element analysis models with formwork restraint described in the previous section. In this section, a simple analytical method was used to calculate stresses expected due to differential camber. Stress predictions using the analytical method were compared with those obtained using finite element analysis.

There are significant similarities between the responses of skewed NEXT beams and standard double-tee beams to torsion. Torsion created in double-tee beams due to uneven supports could be present in NEXT beams due to skew. NEXT beams with higher skew angles have higher differences in camber between the two stems.

The analytical method developed by Banks et al.[16] to analyze double-tee beams under torsion and flexure was used with several modifications to predict the maximum flange bending stress at the ends of NEXT beams with varying skew angles for beam 2. There are differences

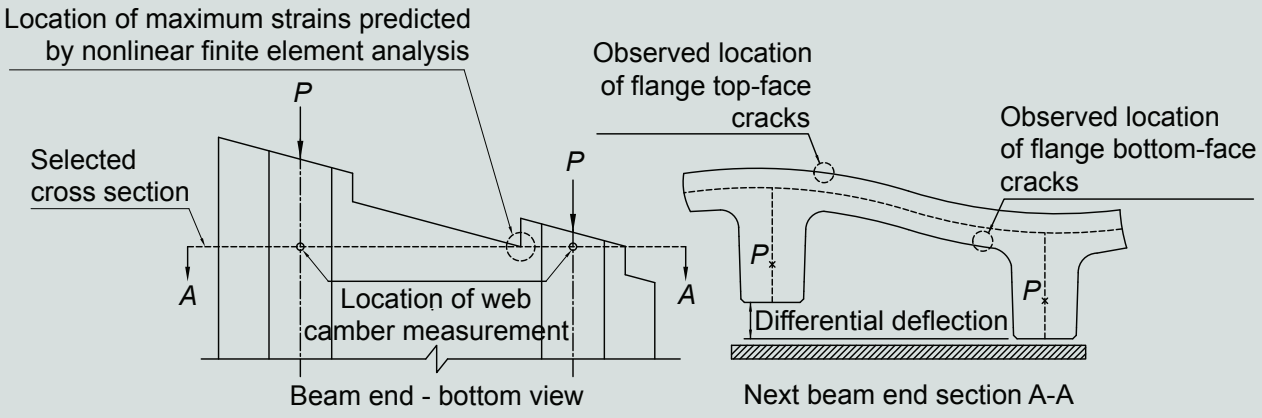

Figure 10. Critical cross section of beam 2 used in analytical calculations and finite element analysis and schematic of differential camber of webs.

Table 3. Comparison of finite element analysis and analytical results of peak flange stresses

Skew angle, degrees	$\sigma_{f.bottom}$, ksi		Finite element analysis/ analytical for $\sigma_{f.bottom}$	$\sigma_{f.top}$, ksi		Finite element analysis/ analytical for $\sigma_{f.top}$
	Finite element analysis	Analytical		Finite element analysis	Analytical	
15	0.889	0.964	0.92	0.25	0.964	0.26
30	1.867	1.715	1.09	0.50	1.715	0.29
45	2.018	2.138	0.94	0.50	2.138	0.23

Note: $\sigma_{f.bottom}$ = flange bottom-face bending stress; $\sigma_{f.top}$ = flange top-face bending stress. 1 ksi = 6.895 MPa.

between the boundary conditions of the double-tee beams assumed by Banks et al. and those of the NEXT beams. To adapt the method to the problem studied in this paper, the NEXT beam was assumed to be supported at midspan (using symmetry boundary conditions along the length of the beam). Therefore, the length of the NEXT beam in the analytical model was assumed to be half the actual length. In addition, in the analytical method developed for double tees, only one bearing point of the beam is uneven with the rest of the bearing points. In the NEXT beams, due to initial camber, the two stems at midspan are higher than the stems at the end. At the end of the beam, the stem on the obtuse side of the beam is at a lower level than the one on the acute side.

The cross section of the beam used to measure maximum bending stress is at the beam end and passes through the region of expected maximum flange bottom-face stresses (Fig. 10, left). Camber for each stem was calculated at the level of the selected cross section, A-A (Fig. 10, left).

According to the method by Banks et al., maximum flange bending stress is a function of section properties and the twist angle experienced by the beam. It can be computed with the following equation:

$$s_f = \frac{6m_{f.max}}{t_f^2}$$

where

$m_{f.max}$ = maximum flange moment per unit length of beam

t_f = flange thickness

σ_f = flange bending stress

The peak flange moment at the end of the beam is obtained with the following equation:

$$m_{f.max} = \frac{6D_{f.eff}}{c_m s} f_d$$

where

$D_{f.eff}$ = effective bending stiffness of flange per unit length of beam

c_m = constant associated with rigid end offset for moment

s = center-to-center web spacing

ϕ_d = twist angle due to distortion of cross section

The previous expression recognizes the increase in flange stiffness at the web–flange intersection by introducing the flange effective stiffness and evaluates the flange moment away from the web–flange centerlines intersection by

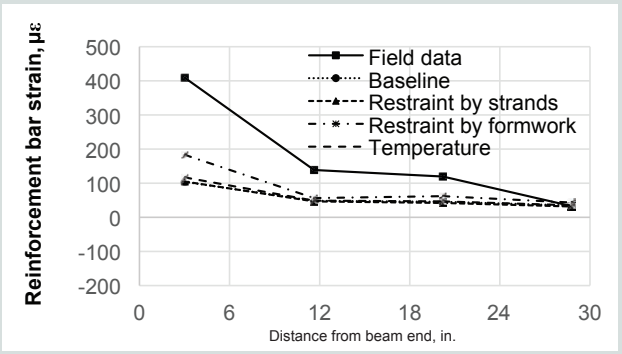

Figure 11. Comparison of reinforcing-bar strains obtained by finite element analysis and instrumentation for beam 2 along gauge line 3. Note: 1 in. = 25.4 mm.

incorporating the rigid end offset constant. The twist angle due to distortion is calculated from the total twist angle of the section, which is equal to the quotient of relative deflection between webs and their spacing. The relative deflection is extracted from known boundary conditions in the problem treated by Banks et al.; however, for the NEXT beam, this must be predicted. In the absence of an analytical tool, the relative deflection was taken from the NEXT beam linear elastic model. In order to use these two equations, some section properties, such as St. Venant's torsion constant and the restraint-of-warping torsion constant, need to be evaluated. Additional details on the procedure can be found elsewhere.[16]

Table 3 summarizes the results from the analytical method[16] and finite element analysis, where positive stresses indicate tension. Because the analytical method is based on linear elasticity, linear elastic finite element analysis was used for comparisons. Peak bending stresses on the flange bottom face $\sigma_{f.bottom}$ correlate well for all skew angles. They also imply that cracks are expected at this location because the theoretical cracking stress for concrete (that is, 0.677 ksi [4.67 MPa]) is exceeded. Alternatively, the analytical method significantly overestimates the flange top-face bending stresses $\sigma_{f.top}$ compared with the linear finite element analysis. The top-face stresses were also shown to be significantly smaller than flange bottom-face stresses obtained by nonlinear finite element analysis. The difference in the results of the analytical model and the finite element analysis can be explained by the differences in the boundary conditions of the double tees and skewed NEXT beams, described earlier.

Other factors

Other factors may contribute to cracking. These factors include sticking of concrete to formwork, shrinkage, and lifting and were out of the scope of this study because they are either impractical or computationally cost-prohibitive to simulate using finite element analysis.

Reinforcing bar stresses

Reinforcing bar strains obtained from the various finite element analysis models of beam 2 were compared with each other and with instrumentation results. **Figure 11** presents a comparison along gauge line 3 only because the instrumentation results indicated very small reinforcing bar strains at gauge lines 1 and 2. Figure 3 shows the locations of the gauge lines.

A comparison of strains along gauge line 3 indicates that the finite element analysis has a qualitative correlation with the instrumentation results. The trend of strain decrease with increasing distance from the beam end is well captured through finite element analysis. The finite element analysis, however, deviates from field measurements when the magnitudes of strains are compared. The lack of quantitative correlation between measurements and finite element analysis is less pronounced for finite element analysis that considers restraint on the beam caused by formwork. The results of the finite element analysis that included prestress and gravity only (the baseline model) and those that included the restraint provided by uncut strands and curing temperatures were essentially the same, indicating a minor contribution of uncut strands or temperature to reinforcing bar stresses.

When formwork is included in the models, the maximum reinforcing bar stresses throughout the beam end reached 19.9 ksi (137 MPa) and were located on the curved bars at the flange–web junction on the exterior side near the acute corner. When only prestress forces are considered, the maximum reinforcing bar stress location was at the bottom transverse and curved bars at the flange–web intersection on the interior side. Consistent with the results of reinforcing bar strains at gauge line 3, inclusion of restraint by strands or temperature stresses during curing did not change the maximum stress magnitude or location. Based on the increase in reinforcing steel stresses with high skew angles shown earlier, inclusion of formwork restraint for beams with high skew will likely cause reinforcing bar stresses higher than 20 ksi (140 MPa), the limit for splitting bar reinforcement stress per 5.10.10 of the AASHTO LRFD specifications.[20]

The lack of a quantitative match between the field instrumentation results and the finite element analysis may be due to several factors. The maximum measured reinforcement strain corresponds to 11.9 ksi (82.1 MPa) of reinforcing bar stress. This value is only 20% of the yield strength of the reinforcing bars and is small. Minor deviations in construction from the plans in reinforcing bar location, gauge location, or orientation may have caused relatively large deviations in this small strain range in the finite element analysis models. Instrumenting a beam at the maximum reinforcing bar stress locations obtained from the model with formwork restraint or instrumenting a beam with a higher skew angle will lead to higher reinforcing bar stresses. This will reduce the high impact of small deviations from construction plans on instrumentation results. In addition, factors that are not practical to simulate using finite element analysis, such as binding to the forms, may be responsible for the difference in the results. Finally, the finite element analysis did not consider curing temperature changes while the beam is restrained. Capturing these effects may improve the finite element analysis results for reinforcing bar stress. For these reasons, at this small skew angle of 15 degrees, the models are deemed to be better suited for evaluating comparative concrete strains than reinforcing bar strains.

Conclusion

Based on the results of this study, the following conclusions can be drawn:

- End-zone concrete stresses created solely by prestressing are not high enough to cause flange cracking in NEXT beams. This is contrary to end-zone stresses in deep bulb-tee beams, indicating that the end-zone behaviors of NEXT beams and bulb-tee beams are different.

- Formwork should be included when NEXT beam ends are simulated or analyzed to investigate detensioning cracks. Cracks are partially due to the restraint on the beam provided by the formwork. Therefore, analyses without formwork will lead to an underestimation of concrete strains and incorrect prediction of the concrete maximum strain and reinforcement maximum stress locations. Alternatively, restraint due to uncut strands and curing temperature stresses alone has a negligible impact on detensioning strains and can be omitted from the analyses.

- Skew causes a differential camber between stems of NEXT beams. This differential camber leads to torsion and transverse bending at the ends and is the largest contributor to end cracks when beams are restrained by formwork. Increases in beam skew angles lead to more severe cracking because larger skew angles increase the differential camber between the two stems of the beam. Skew causes a much higher increase in the flange bottom-face stresses than the flange top-face stresses.

- The torsion method proposed by Banks et al.[16] for double-tee beams can capture the behavior of NEXT beams at one of the most critical locations of the beam (the flange bottom face close to the obtuse corner) when boundary conditions are adjusted for NEXT beams. This confirms that flange cracks on NEXT beams are strongly related to St. Venant's torsion and flange transverse bending.

- Because uneven seating and formwork restraint are significant contributors to cracking, increasing the flexibility of supports during casting, storing, lifting, or creating flange cutouts are recommended to control cracks. Using formwork that can be partially removed before release can also control cracking.

- Additional factors that could be incorporated into analyses to improve the results include coupling of thermal effects, shrinkage, formwork restraint, beam lifting, and sticking of beam to formwork. Implementing a time-dependent concrete stress-strain relationship during curing could improve the results of the thermal analyses.

- Measured reinforcing bar stresses were below 11.9 and 13.3 ksi (82.1 and 91.7 MPa) for the type D beam with a 15-degree skew angle and for the type F beam with a 7.5-degree skew angle, respectively. These stresses are small compared with the yield strength of the reinforcement. Instrumentation of a beam with a higher skew angle at the identified locations of maximum reinforcement stress is recommended to provide better reference data for finite element analysis validation.

- Although not directly assessed in this paper, reinforcing bar stresses for beams with large skew angles and restrained by formwork will likely exceed the serviceability limits of 5.10.10.1 of the AASHTO LRFD specifications[20] for splitting reinforcement (20 ksi [140 MPa]) or 5.9.4.1.2 of the AASHTO LRFD specifications for tension reinforcement (30 ksi [210 MPa]). Additional reinforcing bars should be placed to control reinforcing bar stresses and crack sizes in beams with large skew angles.

- Modified for NEXT beams, the analytical model proposed by Banks et al.[16] can be used to identify NEXT beam skew angle limits, above which flange cracks are expected. This method can also be employed to proportion crack control reinforcement.

Acknowledgments

The authors acknowledge Jersey Precast Corp. in Hamilton, N.J., and L. C. Whitford Materials Co. Inc. in Wellsville, N.Y., for accommodating the research team at their plants for the instrumentation of the beams. The insight of Chad D'Arcy and Larry Crast of L. C. Whitford Materials Co.; Rey Chavez of Jersey Precast Corp.; Michael Hartle, inspector for the NYSDOT; and Michael Twiss of the NYSDOT are particularly acknowledged. The Department of Civil, Structural and Environmental Engineering and Institute of Bridge Engineering at the University at Buffalo in Buffalo, N.Y., provided financial support.

The opinions, conclusions, and results expressed in this paper are the ones of the authors and do not necessarily reflect the views of the individuals, precast concrete companies, transportation agencies, and funding agencies acknowledged here.

References

1. Culmo, M. P., and R. L. Seraderian. 2010. "Development of the Northeast Extreme Tee (NEXT) Beam for

Accelerated Bridge Construction." *PCI Journal* 55 (3): 86–101.

2. Mirza, J. F., and M. E. Tawfik. 1978. "End Cracking in Prestressed Members during Detensioning." *PCI Journal* 23 (2): 66–77.

3. Gergely, P., and M. A. Sozen. 1967. "Design of Anchorage-Zone Reinforcement in Prestressed Concrete Beams." *PCI Journal* 12 (2): 63–75.

4. Arab, A. A., S. S. Badie, and M. T. Manzari. 2011. "A Methodological Approach for Finite Element Modeling of Pretensioned Concrete Members at the Release of Pretensioning." *Engineering Structures* 33 (6): 1918–1929.

5. Okumus, P., M. G. Oliva, and S. Becker. 2012. "Nonlinear Finite Element Modeling of Cracking at the Ends of Pretensioned Bridge Girders." *Engineering Structures* 40: 267–275.

6. Burgueño, R., and Y. Sun. 2011. *Effects of Debonded Strands on the Production and Performance of Prestressed Concrete Beams*. Report RC-1546 for the Michigan Department of Transportation. East Lansing, MI: Michigan State University.

7. Baran, E., C. Shield, C. French, and T. Wyffels. 2004. "Analysis of the Effects of Vertical Pre-release Cracks on Prestressed Concrete Bridge Girders." *PCI Journal* 49 (6): 114–130.

8. Tuan, C. Y., S. A. Yehia, N. Jongpitaksseel, and M. K. Tadros. 2004. "End Zone Reinforcement for Pretensioned Concrete Girders." *PCI Journal* 49 (3): 68–82.

9. Tadros, M. K., S. S. Badie, and C. Y. Tuan. 2010. *Evaluation and Repair Procedures for Precast/Prestressed Concrete Girders with Longitudinal Cracking in the Web*. National Cooperative Highway Research Program report 654. Washington, DC: Transportation Research Board.

10. O'Callaghan, M. R., and O. Bayrak. 2008. *Tensile Stresses in the End Regions of Pretensioned I-Beams at Release*. Technical report IAC-88-5DD1A003-1. Austin, TX: The University of Texas at Austin.

11. Ross, B. E., M. D. Willis, H. R. Hamilton, and G. R. Consolazio. 2014. "Comparison of Details for Controlling End-Region Cracks in Precast, Pretensioned Concrete I-Girders." *PCI Journal* 59 (2): 96–108.

12. Okumus, P., and M. G. Oliva. 2013. "Evaluation of Crack Control Methods for End Zone Cracking in Prestressed Concrete Bridge Girders." *PCI Journal* 58 (2): 91–105.

13. Okumus, P., and M. G. Oliva. 2014. "Strand Debonding for Pretensioned Bridge Girders to Control End Cracks." *ACI Structural Journal* 111 (1): 201–210.

14. Dunkman, D. A., C. G. Hovell, A. M. Moore, A. Avendano, O. Bayrak, and J. O. Jirsa. 2010. "Bursting and Splitting in Pretensioned Concrete Beams." In *2010 fib Congress and PCI Convention and Bridge Conference Proceedings, May 29–June 2, 2010, Washington, D.C.* Chicago, IL: PCI. CD-ROM.

15. Mack, P., G. Force, C. Magnesio, and K. Bryan. 2003. "The Practice of Warping Double Tees." *PCI Journal* 48 (1): 32–48.

16. Banks, G., L. N. Lowes, and J. F. Stanton. 2005. "Analysis and Design for End Effects in Twisted Double Tees." *PCI Journal* 50 (3): 40–59.

17. PCI Committee on Quality Control Performance Criteria. 1983. "Fabrication and Shipment Cracks in Prestressed Hollow-Core Slabs and Double Tees." *PCI Journal* 28 (1): 18–39.

18. PCI Northeast Technical Committee. 2012. *Bridge Member Repair Guidelines*. Report PCINER-01-BMRG. Belmont, MA: PCI Northeast.

19. NYSDOT (New York State Department of Transportation). 2006. *Bridge Manual*. 4th ed. with 2014 revisions. Albany, NY: NYSDOT.

20. AASHTO (American Association of State Highway and Transportation Officials). 2014. *AASHTO LRFD Bridge Design Specifications*. 7th edition. Washington, DC: AASHTO.

21. fib (International Federation for Structural Concrete). 2013. *fib Model Code for Concrete Structures 2010*. Berlin, Germany: Ernst & Sohn.

22. Okumus, P., R. P. Kristam, and M. Diaz Arancibia. 2016. "Sources of Crack Growth in Pretensioned Concrete-Bridge Girder Anchorage Zones after Detensioning." *Journal of Bridge Engineering* 21 (10). doi: 10.1061/(ASCE)BE.1943-5592.0000928.

Notation

c_m = constant associated with rigid end offset for moment

$D_{f.eff}$ = effective bending stiffness of flange per unit length of beam

$m_{f.max}$ = maximum flange moment per unit length of beam

P = prestress load

s = center-to-center web spacing

t_f = flange thickness

Δ = beam deflection

σ_{bottom} = bottom-fiber concrete bending stress

σ_f = flange bending stress

$\sigma_{f.bottom}$ = flange bottom-face bending stress

$\sigma_{f.top}$ = flange top-face bending stress

σ_{top} = top-fiber concrete bending stress

ϕ_d = twist angle due to distortion of cross section

About the authors

Mauricio Diaz Arancibia is a graduate research assistant in the department of Civil, Structural and Environmental Engineering at the University at Buffalo, the State University of New York, in Buffalo, N.Y. He is a student member of PCI.

Pinar Okumus, PhD, is an assistant professor in the department of Civil, Structural and Environmental Engineering at the University at Buffalo, the State University of New York, in Buffalo, N.Y. She is a member of PCI.

Abstract

During prestress release, northeast extreme tee (NEXT) bridge beams crack in their flanges and webs at beam ends in recurrent patterns. These cracks may lead to corrosion in pretensioned and mild reinforcement. Causes of flange cracks in NEXT beams were investigated in this paper using nonlinear finite element analysis that captures stress redistribution in concrete upon cracking and using field measurements of reinforcing bar strains. A torsion-based analytical method was also used to explore the impact of differential camber between stems of skewed beams. The individual contributions of prestress, uncut strand restraint, skew, thermal strains, formwork restraint, and torsion due to differential camber to detensioning cracks were studied. Torsion with formwork restraint and high skew angles were the largest contributors to end cracking. Flange cutouts, flexible supports, or removable formwork are recommended for crack control. The torsion-based method may also be suitable for predicting flange stresses and detailing reinforcement.

Keywords

Beam, detensioning, differential camber, double tee, end cracking, end-zone cracks, finite element analysis, flange cutouts, flange longitudinal cracks, flexible supports, formwork restraint, NEXT beam, northeast extreme tee beam, prestressing, removable formwork, torsion.

Review policy

This paper was reviewed in accordance with the Precast/Prestressed Concrete Institute's peer-review process.

Reader comments

Please address reader comments to journal@pci.org or Precast/Prestressed Concrete Institute, c/o *PCI Journal*, 200 W. Adams St., Suite 2100, Chicago, IL 60606.